


Density distribution in magnetorheological fluid subjected to external forces

Ireneusz Musiałek¹, Karol Musiałek¹, Karol Osowski^{2*} ,
Artur Olszak³, Zbigniew Kęsy¹, Andrzej Kęsy¹

¹ Mechatronics Division, Jan Kochanowski University of Kielce, ul. Żeromskiego 5, 25-369 Kielce, Poland

² Faculty of Mechanical Engineering, Casimir Pulaski Radom University, ul. Malczewskiego 29, 26-600 Radom, Poland

³ Łukasiewicz Research Network – New Chemical Syntheses Institute, al. Tysiąclecia Państwa Polskiego 13a, 24-110 Puławy, Poland

* Corresponding author's e-mail: k.osowski@urad.edu.pl

ABSTRACT

During the operation of hydraulic devices, centrifugal and magnetic forces often affect local density changes in magnetorheological fluid, depending on operating conditions and the composition of the fluid. The density distribution of the magnetorheological fluid in the vessel is measured in order to assess the density changes induced by centrifugal and magnetic forces. Two magnetorheological fluids selected for the tests differ in composition and iron particle size. The density of the magnetorheological fluid is measured in a rotating vessel, and after applying a magnet to a wall of a stationary vessel. During rotation, the magnetorheological fluid is denser near the vessel walls, where the radius of the rotating fluid is the largest. Moreover, it is noted that (both during spinning and after applying the magnet) the density changes of the magnetorheological fluid are not instantaneous, but occur over time.

Keywords: hydraulic devices, magnetorheological fluid, density distribution, magnetic pressure, centrifugal pressure.

INTRODUCTION

Magnetorheological fluids (MR) belong to a group of new working fluids the rheological properties of which can be changed to influence actuator performance. The rheological properties of the MR fluid are modified by changing the intensity of the magnetic field acting on the MR fluid, generated by means of an electric current [1–3]. Therefore, digital control systems can easily be used in actuators containing the MR fluid. This is why MR fluids are used in numerous types of actuators and other devices, such as: viscous clutches and brakes [4–6], hydrodynamic clutches and brakes [7, 8], valves [9–12], dampers [13–15], shock absorbers [16, 17], isolators [18], energy converters [19], landing gears [20] or cantilever beams [21, 22].

The MR fluids are heterogenous fluids consisting of liquid and solid phases. The liquid

phase typically consists of oils, while the solid phase comprises particles of magnetic materials [23, 24]. The MR fluids exposed to a magnetic field have the properties of a non-Newtonian fluid, while in the absence of a magnetic field, they become Newtonian fluids [25].

Actuator designs vary significantly based on the different functions they perform in machines [26, 27]. Consequently, the MR fluid flow varies by application. In viscous clutches and brakes, shear flow occurs with rotational fluid motion, whereas in valves, dampers, clutches, and hydrodynamic brakes, pressure flow occurs, characterized by linear motion. The motion of MR fluid working in actuators is often unsteady. Also, there are different ways of affecting the MR fluid with a magnetic field. Components generating a magnetic field (such as permanent magnets or electromagnet coils) can be stationary [28] or moving

[29]. The magnetic field generated by the AC powered coils can also rotate [30].

Due to the fact that the phases of the MR fluid differ significantly in density and magnetic properties, the external forces acting on the fluid can induce stratification. The phenomenon of separation of two-phase fluids (including MR fluids) under the influence of gravity is called sedimentation and is described by Stoke's law. Higher viscosity of the liquid phase reduces the settling rate of solid particles, which results in a more uniform particle distribution within the vessel [31].

A theoretical analysis based on numerical calculations [32] examines the effect of centrifugal force from the rotation of a vessel containing a two-phase fluid. The assumption is that the two-phase fluid is a non-Newtonian fluid. A power law model with exponent n is used to describe the fluid properties. The continuous finite element method is used in the numerical calculations, and the model solutions are obtained using the "Free-fem++" software. The calculation results show that under vessel rotation, solid particle concentration increases with radius, depends on rotation duration, and is significantly influenced by liquid-phase viscosity. Attractive forces between particles are also significant, particularly for solid particles at the nanoscale. However, under the influence of external forces greater than the attractive forces (such as gravity, buoyancy or centrifugal force) the particles separate.

Article [33] examined changes in the porosity coefficient ξ of iron powder, defined as the ratio of solid particle volume to the volume of space between particles, during rotation in a magnetic field, with the powder dispersed in oil. Static pressure and weight were not taken into consideration. It was assumed that the change in the porosity coefficient is proportional to the pressure dp change, assuming that $d\xi = -a dp$. The proportionality coefficient a is determined experimentally using a specially built test stand. Iron powder was subjected to a magnetic field in a cylinder and compressed by a piston to measure the relationship between piston displacement and applied force. The measurement results show that the value of the coefficient a can range from $-0.30 \times 10^{-3} \text{ cm}^2/\text{g}$ in the absence of a magnetic field to $-0.19 \times 10^{-3} \text{ cm}^2/\text{g}$ in the presence of a magnetic field. It is also calculated that the threshold pressure, caused by centrifugal and magnetic forces, at which the particles agglomerate is 0.25 MPa.

Experimental studies on rotating magnetic field are conducted mainly for ferrofluids the particle sizes of which differ in size from those in the MR fluids. The diameters of solid particles in ferrofluids range from 3 nm to 15 nm, while the diameters of solid particles in MR fluids range from 1 μm to 20 μm [34]. During testing, a vessel containing ferrofluid is placed within coils generating a rotating magnetic field powered by alternating current [35–38]. It was observed that the solid particles of the ferrofluid rotate in the fluid, which causes the fluid to rotate around them at a speed slower than the rotation of particles. Depending on the testing conditions, the solid particle rotation caused the entire ferrofluid to rotate at a slower angular velocity than the magnetic field. The rotation of the entire ferrofluid is caused by inhomogeneity in the following: magnetic field, magnetization, particle concentration, friction coefficient and base fluid viscosity. The angular velocity of the ferrofluid rotation depends on the angular velocity of the magnetic field rotation, the intensity of the magnetic field, the position of the magnetic field relative to the vessel, the number of generating coils, the size of the solid particles and the magnetization of the solid particles. The phenomena occurring in a ferrofluid located in a rotating magnetic field have been explained by the authors in various ways. These include hydraulic interactions of a rotating particle, a phase shift between the magnetization vectors and the magnetic field intensity (causing a rotational torque acting on the particles), and the formation of interacting magnets inside the ferrofluid. The forces that influence these phenomena include magnetic interaction, intermolecular attraction, surface tension, centrifugal force, viscosity, friction, and gravity.

The influence of a rotating magnetic field on the MR fluid placed in a vessel is studied in [39]. In the mounted vessel, ripples appear on the fluid surface immediately after activation of the rotating magnetic field. Subsequently, vortices occur in the MR fluid when the vessel starts to rotate. After increasing the angular velocity of the vessel, the surface of the MR fluid in the vessel assumed a shape similar to a paraboloid of revolution. After switching off the magnetic field, the MR fluid rapidly disperses and flows down the vessel walls. When the vessel containing the MR fluid is immobilized in a rotating magnetic field, a ring of solid particles forms along the vessel walls. The tests also show that solid particles can stick together and form lumps.

During the operation of actuators containing the MR fluid, both fluid rotation and influence of the magnetic field generate external forces, primarily centrifugal and magnetic forces. These forces cause local changes in the composition of the MR fluid, leading to changes in the fluid density. This is why assuming a constant density of the MR fluids in the design calculations of actuators may lead to significant errors.

The article presents experimental studies on the density distribution of two MR fluids during the vessel rotation and after applying a magnet to the wall of a stationary vessel. The described research contributes to increasing the level of knowledge about hydraulic devices with the MR fluid by testing of a density distribution in MR fluid subjected to external forces. The concept of the density distribution testing is innovative. This method has not been used in hydraulic devices with MR.

MATERIALS

Two MR fluids produced internally were used to study the density distribution of fluids under the influence of centrifugal force and magnetic force. The fluids consist of spherical iron particles and silicone oil OL.111, and are marked as A and B. The iron particle diameters and the weight concentration ratio φ of the particles (defined as

the ratio of the mass of solid particles to the mass of silicone oil and solid particles) for fluids A and B were selected to obtain the MR fluids the properties of which would be significantly different. The data on the composition of fluids A and B are summarized in Table 1.

Fluids A and B do not contain additives to limit sedimentation, aggregation and corrosion of iron particles. Due to the significant differences in the composition of the fluids, it would be necessary to supply different amounts of additives, which would render the interpretation of test results difficult.

The images of solid particles of fluids A and B, obtained using a Motic MSZ 140 Series stereomicroscope with halogen illumination, are presented in Figure 1.

METHODS

Method for studying the density distribution of fluids during rotation

The study of the density distribution of fluids during rotation was performed using a test stand consisting of a vessel with the tested MR fluid. The vessel was mounted on the axis of a low-speed electric motor powered by a regulated electric power supply. The test stand is shown in Figure 2.

Table 1. Names and composition of tested MR fluids

Symbol	ρ [g/cm ³]	Weight concentration ratio φ [-]	Volume concentration ratio φ [-]	Fe particle diameter [μ m]
A	2.53	0.67	0.19	3.5 ÷ 6.5
B	2.69	0.75	0.24	100 ÷ 150

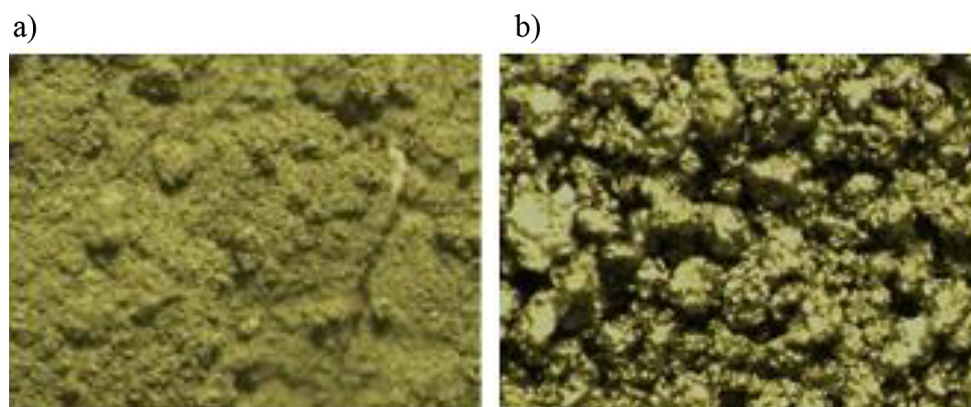


Figure 1. Views of the iron solid particles used to prepare the MR fluids at 50x magnification: a) particles of fluid A, b) particles of fluid B



Figure 2. View of the test stand used to test the density distribution of rotating fluids: 1 – rotating vessel, 2 – low-speed electric motor, 3 – electric power supply

The view of the MR fluid surface during rotation is shown in Figure 3. The diameter of the vessel is 8 cm. During the tests, the rotation speed is increased to a fixed angular velocity ω . After a predetermined rotation time t , the vessel is stopped and a 1 ml fluid sample is withdrawn with a syringe at a selected point along the radius, as presented in Figure 4.

The location of points relative to the vessel wall where the MR fluid is collected is shown in Table 2. The time t_0 of fluid sampling does not exceed 3 seconds, in order to prevent the fluid from l'': fluid weight is obtained by subtracting the weight of the syringe. Dividing the weight of the MR fluid by its volume allows calculating the density ρ of the fluid.

Method of testing the density distribution of a fluid after applying a magnet

Figure 8 shows the test stand designed to study the density distribution of fluids after applying a

magnet to the wall of a stationary vessel. The test stand consists of a vessel equipped with a magnet holder, a neodymium bar magnet measuring $1 \times 2 \times 8$ cm and an SMS102 induction meter.

After filling the vessel with a MR fluid and applying the magnet in a selected position, approximately 1 cm^3 of the MR fluid was collected from the vessel using a syringe. The locations of the points where the MR fluid was sampled, as well as the mean induction value B at these points, are presented in Figure 9 and Table 3.

The average value of induction B is assumed to be the same for the tested fluids, due to the fact that the induction B values measured for these MR fluids at the same point are very similar, differing just by a few percent.

Subsequently, the syringe was weighted, and the fluid weight was obtained by subtracting the weight of the syringe. Dividing the weight of the MR fluid by its volume allows calculating the density.

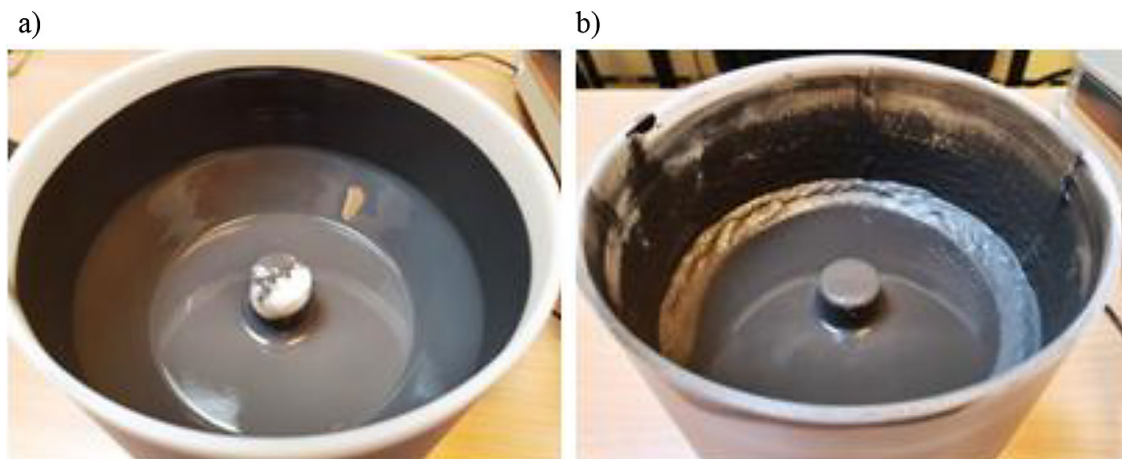


Figure 3. The view of the MR fluid surface during 20-minute rotation: a) fluid A, b) fluid B

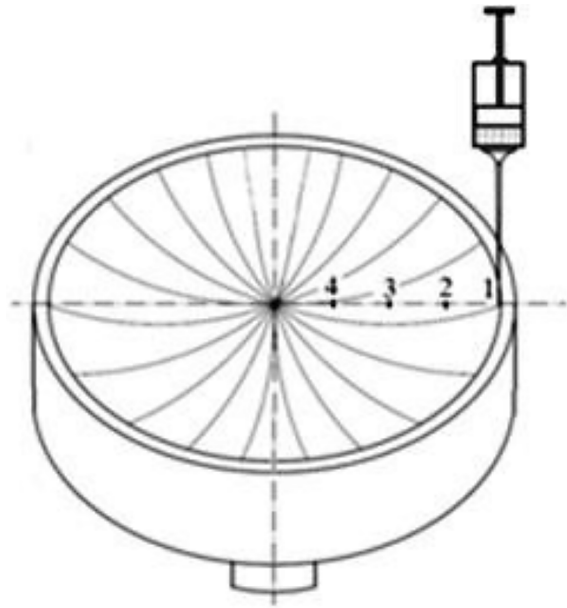


Figure 4. Method of collecting MR fluid

RESULTS

Density distribution tests

Figure 5 shows density changes in MR fluids A and B depending on the distance l of the sample collection point from the edge of the vessel, after 5 minutes of rotation at angular velocity $\omega = 6$ rad/s. At this angular velocity the MR fluid did not yet spill out of the vessel during rotation.

Figure 6 shows changes in density near the vessel wall (for $l = 0$ cm) for fluids A and B, depending on rotation time t at an angular velocity $\omega = 6$ rad/s.

Table 2. Location of fluid collection points

Point	Distance l from the vessel's edge [cm]	Point radius [cm]
1	0	1
2	1	3
3	2	2
4	3	1

Pressure caused by centrifugal force

The pressure due to the centrifugal force p_o [Pa] at a selected point can be calculated as [40]:

$$p_o = 0.5\rho\omega^2r^2 \quad (1)$$

where: ρ – MR fluid density [kg/m³], ω – angular velocity [rad/s], r – radius [m].

Figure 7 shows the relationship between centrifugal pressure p_o and vessel radius r , calculated for fluids A and B using Equation 1 and density values from Figure 5.

Results of the fluid density distribution after applying a magnet

Figure 10 shows density changes depending on the distance l of the sampling point from the vessel wall, for fluids A and B, 5 minutes after applying the magnet to the vessel wall.

Figure 11 shows density changes depending on induction B measured at sampling points for fluids A and B, 5 minutes after applying the magnet. Figure 12 shows changes in density near the vessel wall ($l = 0$ cm) for fluids A and B, in relation to time after magnet application.

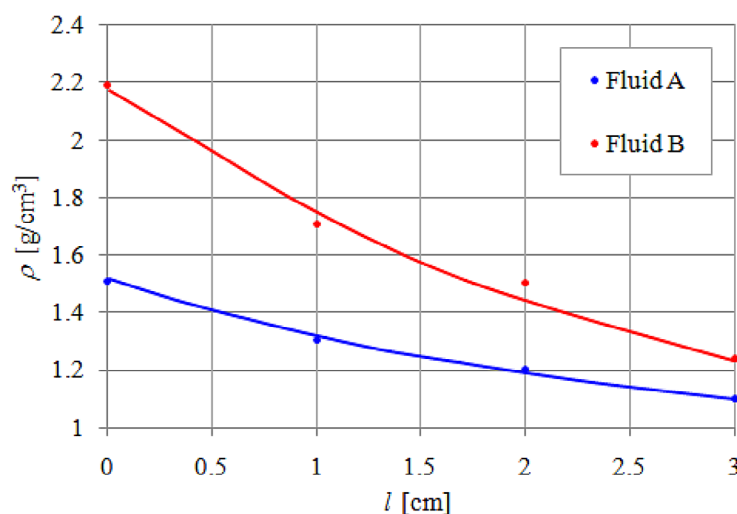


Figure 5. Changes in ρ depending on l after 5 minutes of rotation

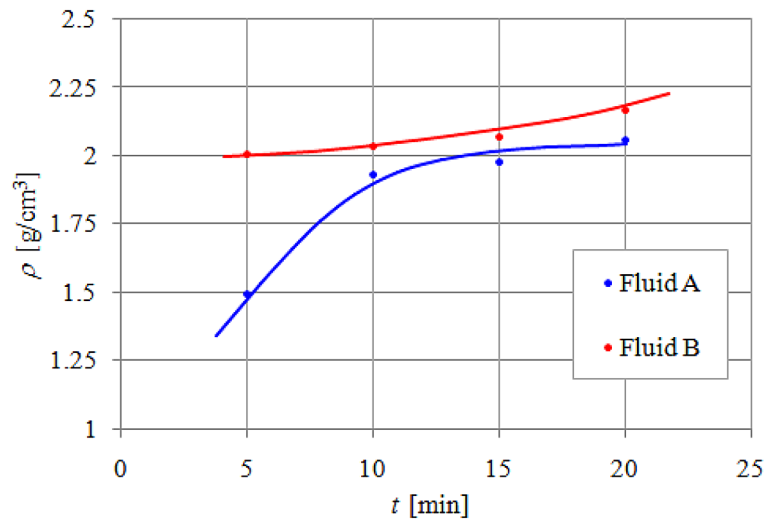


Figure 6. Density ρ in relation to rotation time t of fluids A and B near the vessel wall ($l = 0$ cm)

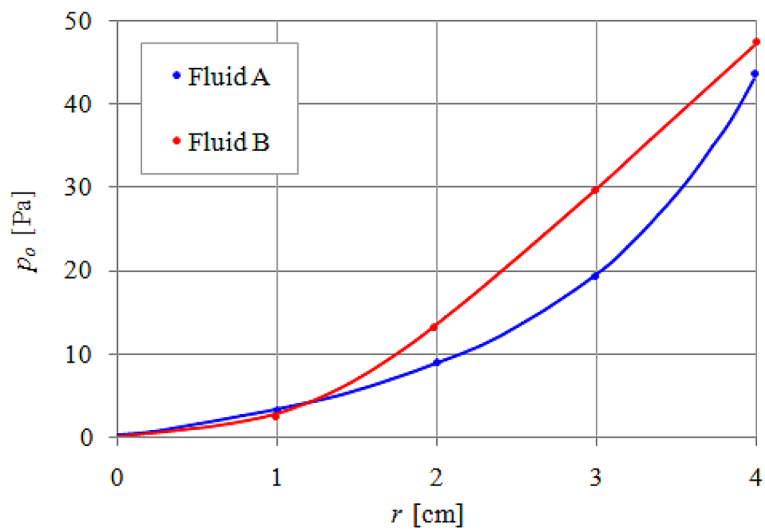


Figure 7. Pressure p_0 in relation to the vessel's radius r for fluids A and B, $\omega = 6$ rad/s



Figure 8. Test stand for testing the density distribution after magnet application: 1 – vessel equipped with a magnet holder, 2 – neodymium bar magnet, 3 – induction meter, 4 – measuring probe

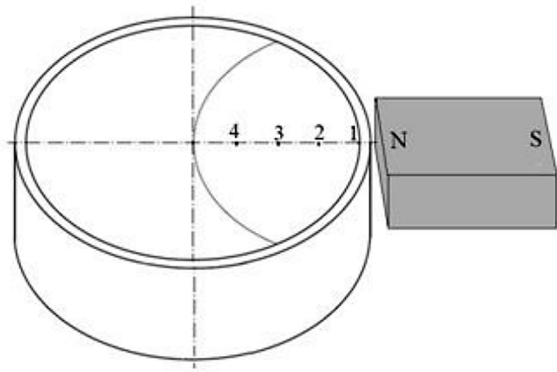


Figure 9. Location of collecting points for MR fluid

The view of the MR fluid after applying a bar magnet to the vessel wall is shown in Figure 13. Figure 14 shows the view of the MR fluid in the presence of a magnetic field.

Magnetic pressure

The magnetic pressure p_m [Pa] in the MR fluid caused by the presence of a magnetic field at a selected point can be calculated on the basis of formula [41, 42]:

$$p_m = B^2 / 2\mu_0\mu_r \quad (2)$$

where: B – magnetic induction [T], $\mu_0 = 4\pi \times 10^{-7}$ H/m – vacuum magnetic permeability, μ_r – relative magnetic permeability of MR fluid [-].

On the basis of reference [43] the relative magnetic permeability μ_r for both tested fluids is assumed to be 2.7. Figure 15 shows the dependence of pressure p_m , caused by the magnetic field, on the vessel radius r , calculated using formula (2) and of magnetic induction values from Table 3.

Measurement errors

The relative error δ_p of determining the MR fluid density during rotation and determining the density during interaction with a magnetic field (after magnet application) is calculated on the basis of formula [44]:

$$\delta_p = \frac{1}{g} \sqrt{\sum_{j=1}^k \left(\frac{\partial g}{\partial x_j} \right)^2 (s_j)^2} \quad (3)$$

where: $g = f(x_1, \dots, x_k)$ – a complex physical quantity calculated from k measured quantities x_1, \dots, x_k , s_j – measurement uncertainty x_j .

Table 3. Locations of collecting points of MR fluids and mean induction B values

Point	Distance l from the vessel's edge [cm]	Radius [cm]	Mean induction B at the point [mT]
1	0	4	221.2
2	1	3	27.7
3	2	2	6.1
4	3	1	2.2

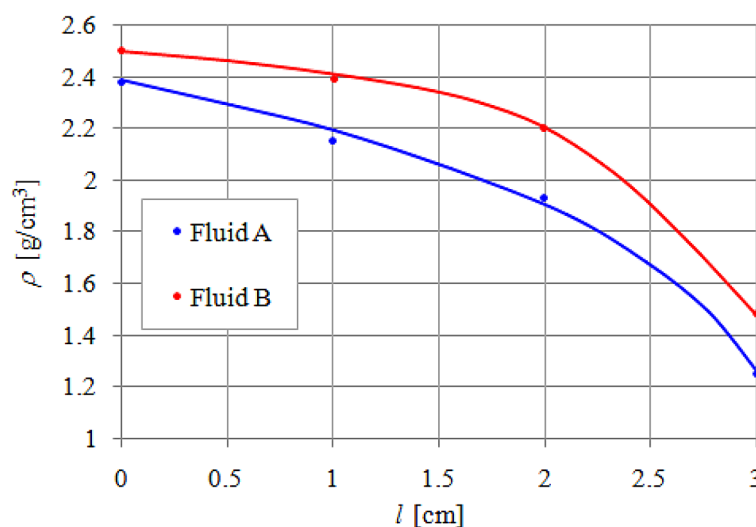


Figure 10. Changes in ρ in relations to l , 5 minutes after applying the magnet

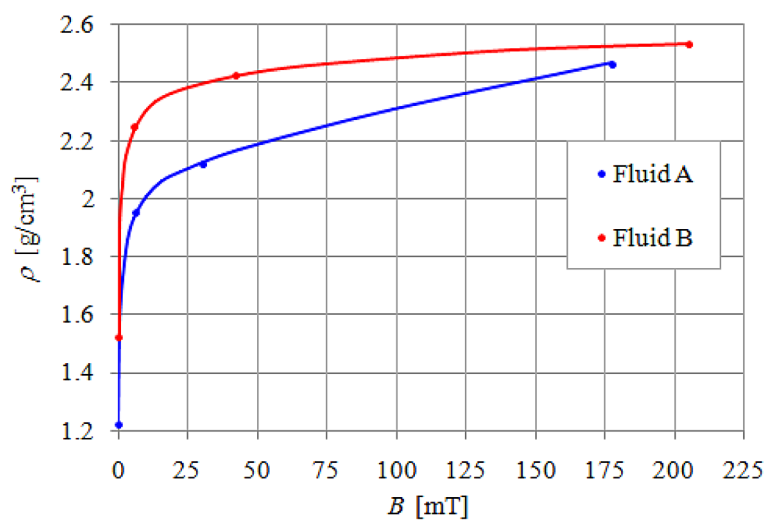


Figure 11. Changes in ρ in relations to B , 5 minutes after applying the magnet

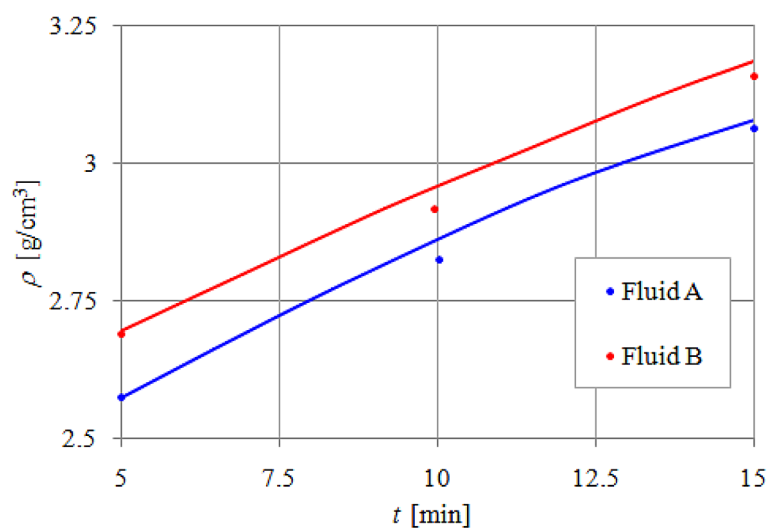


Figure 12. Changes in ρ in relations to magnet application time for fluids A and B at point 1 for $B = 221.2$ mT

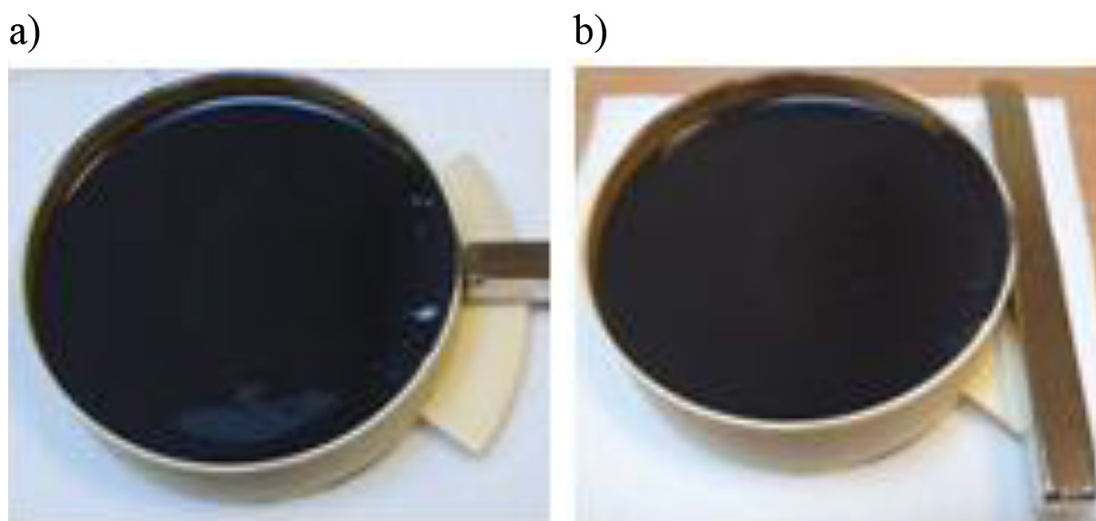


Figure 13. View of fluid A after magnet application: a) perpendicular to the vessel wall, b) parallel to the vessel wall

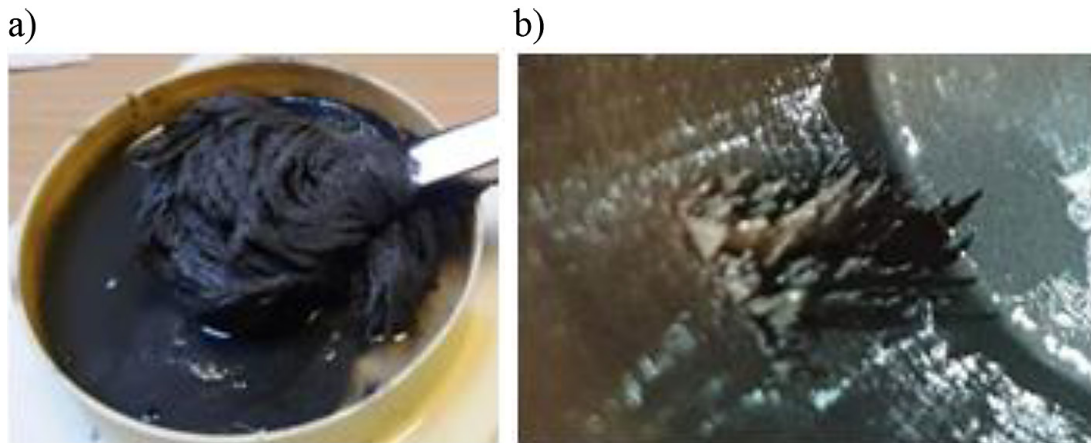


Figure 14. Effect of a magnetic field on the MR fluid: a) fluid B after direct contact with the pole of a bar magnet, b) spikes formed from a small amount of fluid A near the pole of a bar magnet

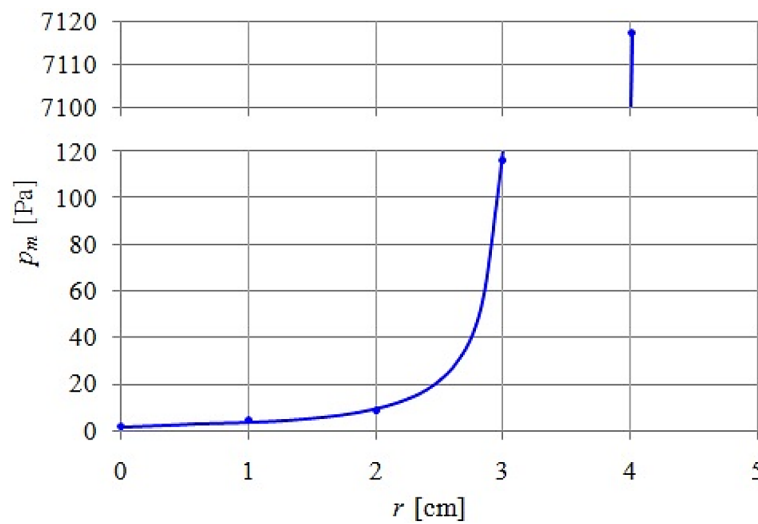


Figure 15. Pressure p_m in relation to vessel radius r for fluid A, $\omega = 6$ rad/s

For density ρ , the function g is written as follows:

$$g = \rho = \frac{m}{V} = \frac{x_1}{x_2} \quad (4)$$

where: $m = x_1$ – weight of the MR fluid sample [g], $V = x_2$ – volume of the MR fluid sample [ml].

After taking into consideration (4) in (3), the obtained equation is:

$$\delta_\rho = \frac{1}{g} \sqrt{\left(\frac{1}{x_2}\right)^2 (s_1)^2 + \left(\frac{x_1}{x_2^2}\right)^2 (s_2)^2} \quad (5)$$

where: $x_1 = m$ – weight of the MR fluid sample [g], $x_2 = V$ – volume of the MR fluid sample [ml].

The measurement uncertainty s is assumed to be 0.5 measurement division, Table 4. As a result of calculations performed on the basis of formula (5) it was found that the errors δ_ρ for all determined density values ρ do not exceed 5%.

The relative error caused by the time it takes to collect the sample for density estimation of the MR fluid is calculated according to the formula:

$$\delta_t = \frac{\Delta}{\rho} = \frac{v \cdot t_0}{\rho} \quad (6)$$

where: Δ – density change over time t_0 [g/cm³],
 v – rate of change of density [g/cm³s],
 t_0 – MR fluid sampling time [s].

Rates of density change v of the MR fluids obtained on the basis of Figure 6 and Figure 12 are shown in Table 5.

Table 4. Data for error calculation δ_p for determined values ρ

Force	MR fluid	x_1 [g]	s_1 [g]	x_2 [ml]	s_2 [ml]
Centrifugal	A	$1.2 \div 1.5$	0.05	1.0	0.05
	B	$1.3 \div 2.1$	0.05	1.0	0.05
Magnetic	A	$1.2 \div 2.5$	0.05	1.0	0.05
	B	$1.4 \div 2.6$	0.05	1.0	0.05

On the basis of the calculations performed using formula (4), it was found that for all determined values of density ρ , errors δ_i did not exceed 1 %.

DISCUSSION

Both during rotation and after magnet application, the solid particles in the MR fluids move in the direction of centrifugal and magnetic forces, leading to changes in fluid density ρ . In the case of centrifugation, the MR fluid density is higher near the vessel walls, i.e. where the radius r of the rotating vessel is the largest. When exposed to a magnetic field, the MR fluids are most dense where the magnetic induction B is the highest, i.e. at the point where the magnet pole is applied to the vessel wall. Density changes also occurred over time, both during rotation and in the presence of a magnetic field.

Figure 3 also shows that the surface of fluid A (containing particles of smaller diameter) is smooth during rotation, which indicates that stratification does not occur. However, fluid B stratified during rotation, as indicated by its wavy surface and accumulation of particles mainly at the vessel wall, where the centrifugal forces were the greatest.

Figure 5 shows that during rotation, density ρ decreases parabolically, depending on the distance l of the point from the vessel's edge. The changes in the MR fluid density ρ over time t , shown in Figure 6, also follow a roughly parabolic pattern. Initially, the density of fluid A increases more quickly, while the changes in fluid B occur more slowly. The reason for this course

of changes in the MR fluid density ρ is the size difference between particles in fluid A and fluid B. The particles of fluid A move faster due to their smaller diameter, so the density increases faster near the vessel walls. As shown in Figures 5 through 6, which present the rotation of MR fluids A and B, the density ρ values are lower for fluid A than for fluid B. This is due to the lower iron particle content in fluid A. For fluids A and B, the dependence of the pressure p_o caused by the centrifugal force on the radius r of the vessel does not change parabolically (as it does for single-phase fluids). As shown in Figure 7, the dependence is described by a fourth-degree polynomial. For the tested fluids A and B, the fluid density after magnet application increases the closer it is to the vessel wall. The same is true for the rotation of MR fluids, as shown in Figure 10. However, the curves connecting the sampling points in Figure 10 are convex. The inclination angle of these curves increases with distance from the vessel walls. Figure 11 show that the course of density change ρ with respect to magnetic induction B is strongly non-linear for both fluids. The density begins a rapid decrease for induction B values below 50 mT. However, it should be noted that the dependence of the induction B on the distance l is also strongly non-linear, as shown in Table 3. Figure 12 shows that the course of density change ρ over time t is nearly linear. Similarly as in the case of rotation, the density values ρ , as shown in Figures 10 through 12, are smaller for fluid A than fluid B due to lower iron particle content.

Figure 13 shows that accumulation of solid particles near the magnet pole causes the MR fluid level to rise at the vessel walls, similarly to

Table 5. Error calculation data δ_i for determined values of ρ

Force	MR fluid	v [g/cm ³ s]	t_0 [s]
Centrifugal	A	$3.3 \times 10^{-4} \div 9.7 \times 10^{-4}$	3
	B	$2.4 \times 10^{-4} \div 2.6 \times 10^{-4}$	3
Magnetic	A	$8.4 \times 10^{-4} \div 9.9 \times 10^{-4}$	3
	B	$6.6 \times 10^{-4} \div 9.4 \times 10^{-4}$	3

what happens when the fluid rotates. The influence of the solid particle size on the fluid behavior in the presence of a magnetic field is shown in Figure 14. It can be seen that the particles of fluid A are arranged along the magnetic field lines in spikes characteristic of typical MR fluids, while the particles of fluid B are separated from the oil. As it can be seen from Figure 15, the change in the magnetic pressure p_m depending on the radius r of the vessel is also strongly non-linear.

CONCLUSIONS

The following conclusions can be drawn from the results of the experimental studies:

1. The action of external forces, such as centrifugal and magnetic forces, cause density distribution in the MR fluid. These changes do not occur instantly but develop over time.
2. The density changes in the tested fluids under the influence of centrifugal and magnetic forces are similar. The differences in the behavior of fluids A and B are related to the amount and size of solid particles. For fluid B, containing a larger mass of solid particles, the density changes are greater than for fluid A.
3. A significant difference in the behavior of MR fluids during rotation, compared to typical single-phase fluids, is a result of the dependence of the pressure induced by centrifugal force on the radius of rotation. The equation describing this relationship for single-phase fluids is a second-degree polynomial, whereas for the MR fluids it is a fourth-degree polynomial.
4. Changes in density and magnetic pressure in the MR fluid depend only on magnetic induction and, when a magnet is applied to the vessel wall, are strongly non-linear.
5. Measurement errors related to the performed tests are less than 5%.

REFERENCES

1. Mendes G., Goldasz J., Ferreira Â. Model-based prototyping of a controller for MR actuators. 24th International Carpathian Control Conference (ICCC) 2023; 93–98. <https://doi.org/10.1109/ICCC57093.2023.10178923>
2. Takesue N., Furusho J., Kiyota Y. Fast response MR-fluid actuator. JSME International Journal Series C 2004; 47(3): 783–791.

3. Oh J. S., Sohn J. W., Choi S. B. Applications of magnetorheological fluid actuator to multi-DOF systems: State-of-the-art from 2015 to 2021. *Actuators* 2022; 11(2): 1–24. <https://doi.org/10.3390/act11020044>
4. Kluszczyński K. and Pilch Z. The choice of the optimal number of discs in an MR clutch from the viewpoint of different criteria and constraints. *Energies* 2021; 14(21): 1–13. <https://doi.org/10.3390/en14216888>
5. Yang Z. Q., Kermani M. R. A. Computationally efficient hysteresis model for magneto-rheological clutches and its comparison with other models. *Actuators* 2023; 12(5): 1–18. <https://doi.org/10.3390/act12050190>
6. Spotowski T., Osowski K., Musiałek I., Olszak A., Kęsy A., Kęsy Z., Choi S. B. A feedback control sensing system of an electrorheological brake to exert a constant pressing force on an object. *Sensors* 2023; 23(15): 1–20. <https://doi.org/10.3390/s23156996>
7. Kęsy Z. and Kęsy A. Prospects for the control of a torque converter using magnetic fluid. *IEE International Colloquium - Innovative Actuators for Mechatronic Systems* 1995; 170: 10/1–10/3. <https://doi.org/10.1049/ic:19951054>
8. Olszak A., Osowski K., Kęsy Z., Kęsy A. Investigation of hydrodynamic clutch with MR fluid. *J. Intell. Mater. Syst. Struct.* 2018; 30(1): 155–168. <https://doi.org/10.1177/1045389X1880346>
9. Milecki A., Jakubowski A., Kubacki A. Design and control of a linear rotary electro-hydraulic servo drive unit. *Appl. Sci.* 2023; 13(15): 1–11. <https://doi.org/10.3390/app13158598>
10. Hu G., Liao M., Li W. Analysis of a compact annular-radial orifice flow magnetorheological valve and evaluation of its performance. *J. Intell. Mater. Syst. Struct.* 2017; 28(10): 1322–1333. <https://doi.org/10.1177/1045389X16672561>
11. Hu G., Long M., Huang M., Li W. Design, analysis, prototyping, and experimental evaluation of an efficient double coil magnetorheological valve. *Adv. Mech. Eng.* 2014; 6: 1–9. <https://doi.org/10.1155/2014/403410>
12. Salloom M. Y. and Almuhanha M. Y. Design and analysis of magneto-rheological relief valve using a permanent magnet. *Advances in Science and Technology Research Journal* 2025; 19(1): 243–255. <https://doi.org/10.12913/22998624/195494>
13. Ahamed R., Ferdaus M. M., Li, Y. Advancement in energy harvesting magneto-rheological fluid damper: A review. *Korea-Aust Rheol J.* 2016; 28(4): 355–379. <https://doi.org/10.1007/s13367-016-0035-2>
14. Gołdasz J., Sapiński B. Nondimensional characterization of flow-mode magnetorheological fluid dampers. *J. Intell. Mater. Syst. Struct.* 2012; 23(14): 1545–1562. <https://doi.org/10.1177/1045389X12447293>

15. Solepatil S. B., Mali A. S., Dive V., Kolekar A. B. Design, development, and performance analysis of a magnetorheological damper for piping vibration control. *Advances in Science and Technology Research Journal* 2025; 19(5): 344–355. <https://doi.org/10.12913/22998624/202537>
16. Milecki A., Sedziak D., Ortmann J., Hauke M. Controllability of MR shock absorber for vehicles. *Int. J. Veh. Des.* 2005; 38(2): 222–233. <https://doi.org/10.1504/IJVD.2005.007294>
17. Gołdasz J. and Sapinski B. *Insight into magnetorheological shock absorbers*; Springer International Publishing: Cham, Switzerland, 2015; 1–251.
18. Priyandoko G., Hunaini F., Imaduddin F., Ubaidillah U., Suwandono P., Sasongko M. I. N. Development of a vibration isolator on the basis of a magneto-rheological elastomer. *Advances in Science and Technology Research Journal* 2024; 18(8): 272–280. <https://doi.org/10.12913/22998624/194441>
19. Lo Sciuto G., Bijak J., Kowalik Z., Kowol P. Magnetorheological fluid magnetic spring harvester design and characterization. *Advances in Science and Technology Research Journal* 2025; 19(5): 128–141. <https://doi.org/10.12913/22998624/200857>
20. Stalin S. S., Uthayakumar M., Balamurugan P., Pethuraj M., Śladek J. A., Niemczewska-Wójcik M. Synthesis of silicone oil based magnetorheological fluid and performance analysis in a landing gear using bat-based gradient boost mechanism. *Advances in Science and Technology Research Journal* 2025; 19(5): 375–389. <https://doi.org/10.12913/22998624/202704>
21. Lara-Prieto V., Parkin R., Jackson M., Silberschmidt V., Kęsy Z. Vibration characteristics of MR cantilever sandwich beams: experimental study. *Smart Mater. Struct.* 2009; 19(1): 1–9. <https://doi.org/10.1088/0964-1726/19/1/015005>
22. Oh H. U. and Onoda J. An experimental study of a semiactive magneto-rheological fluid variable damper for vibration suppression of truss structures. *Smart Mater. Struct.* 2002; 11(1): 156–162. <https://doi.org/10.1088/0964-1726/11/1/318>
23. Fertman V. E. *Magnetic fluids guidebook: Properties and applications*. Hemisphere Publishing Corporation, 1990.
24. Sapiński B. and Horak W. Rheological properties of MR fluids recommended for use in shock absorbers. *Acta Mech. Autom.* 2013; 7(2): 107–110. <https://doi.org/10.2478/ama-2013-0019>
25. Genc S. and Phule P. P. Rheological properties of magnetorheological fluids. *Smart Mater. Struct.* 2002; 11(1): 140–146. <https://doi.org/10.1088/0964-1726/11/1/316>
26. Do X. P. and Choi S. B. Magnetorheological fluid based devices reported in 2013–2018: Mini-review and comment on structural configurations. *Front. Mater.* 2019; 6: 1–8. <https://doi.org/10.3389/fmats.2019.00019>
27. Ahamed R., Ferdaus Md M., Li Y. Advancement in energy harvesting magneto-rheological fluid damper: A review. *Korea-Australia Rheology Journal* 2016; 28(4): 355–379. <https://doi.org/10.1007/s13367-016-0035-2>
28. Sapiński B., Węgrzynowski M., Nabielec J. Magnetorheological damper-based positioning system with power generation. *J. Intell. Mater. Syst. Struct.* 2017; 29(6): 1236–1254. <https://doi.org/10.1177/1045389X17730928>
29. Bucchi F., Forte P., Frendo F. Analysis of the torque characteristic of a magnetorheological clutch using neural networks. *J. Intell. Mater. Syst. Struct.* 2014; 26(6): 680–689. <https://doi.org/10.1177/1045389X14546654>
30. Rosenseig, R. E. *Ferrohydrodynamics*; Cambridge University Press: Cambridge, UK, 1985; 344.
31. Choi S. B. Sedimentation stability of magnetorheological fluids: The state of the art and challenging issues. *Micromachines* 2022; 13(11): 1–22. <https://doi.org/10.3390/mi13111904>
32. Zheng L., Li B., Lin P., Zhang X., Zhang C., Zhao B., Wang T. Sedimentation and precipitation of nanoparticles in power-law fluids. *Microfluid and Nanofluid* 2012; 15(1): 11–18. <https://doi.org/10.1007/s10404-012-1117-1>
33. Vorobyeva, T. M. *Electromagnetic clutches and couplings*; Pergamon Press: Oxford, 1965; 82.
34. Vékás L. Ferrofluids and magnetorheological fluids. *Advances in Science and Technology* 2008; 54: 127–136. <https://doi.org/10.4028/www.scientific.net/AST.54.127>
35. Mailfert L. and Martinet A. Flow regimes for a magnetic suspension under a rotating magnetic field. *J. Phys.* 1974; 34: 197–201. <https://doi.org/10.1051/jphys:01973003402-3019700>
36. Rosenthal A. D., Rinaldi C., Franklin T., Zahn M. Torque measurements in spin-up flow of ferrofluids. *J. Fluids Eng. Trans. ASME* 2004; 126(2): 196–205. <https://doi.org/10.1115/1.1669030>
37. Moskowitz R. and Rosensweig R. E. Nonmechanical torque-driven flow of a ferromagnetic fluid by an electromagnetic field. *Appl. Phys. Lett.* 1967; 11: 301–303.
38. Anton I., Vekas L., Potencz I., Suciu E. Ferrofluid flow under the influence of rotating magnetic fields. *IEEE Trans. Magn.* 1980; 16: 283–287. <https://doi.org/10.1109/TMAG.1980.1060612>
39. Musiałek K., Musiałek I., Osowski K., Olszak A., Mikulska A., Kęsy Z., Kęsy A., Choi S. B. A New type of hydraulic clutch with magnetorheological fluid: Theory and experiment. *Micromachines* 2024; 15(5): 1–17. <https://doi.org/10.3390/mi15050572>

40. Dixo S. L. and Hall C. Fluid Mechanics and thermodynamics of turbomachinery, 7th ed.; Elsevier, US, 2013; 537.
41. Zborowski M., Moore L. R., Williams P. S., Chalmers J. J. Magnetic pressure as a scalar representation of field effects in magnetic suspensions. *AIP Conf Proc.* 2010; 1311(1): 111–117. <https://doi.org/10.1063/1.3529999>
42. Purwadi J. W., Eko P. B., Ubaidillah U., Fitriani I. Magnetically-induced pressure generation in magnetorheological fluids under the influence of magnetic fields. *Appl. Sci.* 2021; 11(21): 1–20. <https://doi.org/10.3390/app11219807>
43. Žáček J., Strecker Z., Jeniš F., Macháček O., Goldasz J., Sapinski B., Vrbka M., Kubík M. Impact of magnetorheological fluid composition on their behaviour in gradient pinch mode. *Sci. Rep.* 2024; 14: 1–14. <https://doi.org/10.1038/s41598-024-82752-6>
44. Kesy Z. Modeling and testing of electrorheological and magnetorheological working fluids; Politechnika Radomska, Poland, 2009; 229 (in Polish).